Nonlinear Dynamics **10:** 1–18, 1996.

The Dynamics of a Bouncing Ball with a Sinusoidally Vibrating Table Revisited

ALBERT C. J. LUO and RAY P. S. HAN
Department of Mechanical & Industrial Engineering, University of Manitoba, Winnipeg, Manitoba, Canada R3T 2N2

(Received: 1 April 1994; accepted: 19 April 1995)

Abstract. The dynamical behavior of a bouncing ball with a sinusoidally vibrating table is revisited in this paper. Based on the equation of motion of the ball, the mapping for period-1 motion is constructed and thereby allowing the stability and bifurcation conditions to be determined. Comparison with Holmes's solution [1] shows that our range of stable motion is wider, and through numerical simulations, our stability result is observed to be more accurate. The Poincaré mapping sections of the unstable period-1 motion indicate the existence of identical Smale horseshoe structures and fractals. For a better understanding of the stable and chaotic motions, plots of the physical motion of the bouncing ball superimposed on the vibration of the table are presented.

Key words: Bouncing ball, vibrating table, stability and bifurcation, period-1 motion.

Introduction

Holmes [1] can be credited as the first person to systematically study the nonlinear dynamics of a ball bouncing vertically on a sinusoidally vibrating table. The ball was considered small compared to the massive table and thus, the motion of the table was not affected by the repeated impacts of the ball. He also assumed that the distance traveled by the free-falling ball between impacts is large compared to the overall displacement of the table and proceeded to give an approximate equation for the time interval between impacts. On the basis of this model, he arrived at a simple difference equation which he used to demonstrate the various periodic and non-periodic motions and other chaotic phenomena. In our opinion this simplified model based on a discrete mapping approach is unnecessary and in some respect, inadequate. We will present a model that is based on the equation of motion of the ball.

Impact motion exists in a wide spectrum of engineering applications, ranging from moored ships undergoing repeated contacts with fenders to moving parts in machinery and fluid induced vibration in tubes. An engineer is not only concerned with the wear and fatigue generated by the impacting system, but also the undesirable noise level that accompanies such motion. A simple model of this discontinual system is to employ a single degree-of-freedom impact oscillator. This deceptively simple model can exhibit an amazingly rich variety of nonlinear behaviors [1–7]. Wood and Byrne [3] presented an interesting analysis of a randomly repeated impacting process and hinted that such random non-periodic motion apparently exist even when the system is forced by sinusoidal excitations. This motivated Holmes [1] to launch an investigation into the problem. Everson [4] investigated the chaotic response of a bouncing ball using a model similar to Holmes's. Other studies related to the dynamics of a bouncing ball are the motion of impact dampers [8–15].

In this paper, the dynamics of a bouncing ball impacting on a harmonically excited massive table is revisited. Unlike Holmes [1], our model is based on the differential equation of motion

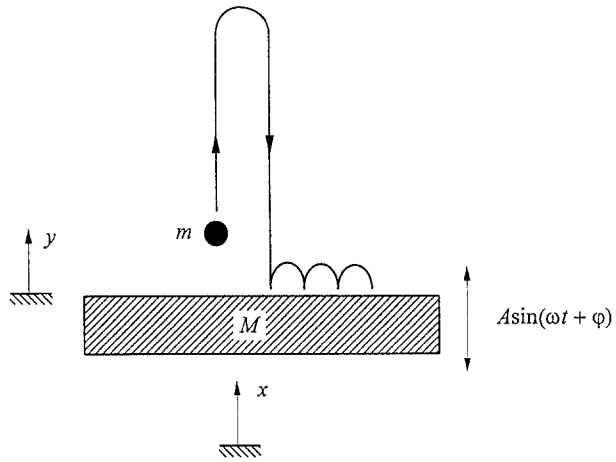

Fig. 1. Mechanical model of the bouncing ball with a vibrating table.

of the ball and from this, an appropriate mapping (or switch plane) is constructed. Also, we did not have to assume that the distance traversed by the free-falling ball is large compared to the motion of the table and this enables us to model large amplitude excitations. Accordingly, our computed time interval between impacts is exact, whereas it was approximate in Holmes. The stability and bifurcation conditions of the system are derived and presented here. To verify the results, numerical simulations are carried out. The focus of this paper is only on period-1 motion, with the more general period-n motion report currently under preparation [16].

Equation of Motion, Discontinual Subsets and Poincaré Mapping

Figure 1 depicts the mechanical model of a bouncing ball m moving freely in the vertical direction with a vibrating table of mass M. It is assumed that the table is massive compared to the ball and therefore, the motion of the table is not affected by the repeated impacts of the bouncing ball, i.e. $m \ll M$. As in the work of Holmes [1], the external excitation, namely, the motion of the table, is taken to be that of the simple harmonic motion. That is,

$$E = A\sin(\omega t + \varphi), \tag{1}$$

where A, ω and φ are the forcing amplitude, the forcing frequency and the initial phase angle.

Denoting the absolute and relative (to the table) displacements of the ball by x, y respectively, and if $(\dot{})$ represents time derivatives, we have

$$\begin{aligned} x &= y + E(t, A) \\ \dot{x} &= \dot{y} + \dot{E}(t, A) \\ \ddot{x} &= \ddot{y} + \ddot{E}(t, A). \end{aligned} \tag{2}$$

Substituting Equation (1) into Equation (2) and considering gravity but neglecting friction, yields the equation of motion in the relative coordinate system:

$$\ddot{y} = A\omega^2 \sin(\omega t + \varphi) - g, \tag{3}$$

where g is the gravity acceleration. Integrating Equation (3) and invoking initial conditions $(y_0, \dot{y}_0)$, the velocity and displacement of the ball are

$$\dot{y} = -A\omega\cos(\omega t + \varphi) - gt + [\dot{y}_0 + gt_0 + A\omega\cos(\omega t_0 + \varphi)] \tag{4}$$

$$y = -A\sin(\omega t + \varphi) - \frac{1}{2}gt^2 + [\dot{y}_0 + gt_0 + A\omega\cos(\omega t_0 + \varphi)](t - t_0) + A\sin(\omega t_0 + \varphi) + \frac{1}{2}gt_0^2 + y_0. \tag{5}$$

For a system with discontinuities such as the impact problem here, all results concerning the existence, stability and bifurcation of periodic solutions of a nonlinear system are, with some modifications, directly applicable (Reithmeier [7]). The discontinuities caused by the impacts between the ball and the table imply that the state-space of the bouncing ball can be divided into many continuous subsets X_i. For the subset between the ith and $(i+1)$th impacts, the values of the ith impact just after the impact can be chosen as initial conditions for X_i. This subset can be determined from Equations (4)–(5) as

$$\dot{y} = -A\omega\cos(\omega t + \varphi) - gt + [\dot{y}_i^+ + gt_i + A\omega\cos(\omega t_i + \varphi)] \tag{6}$$

$$y = -A\sin(\omega t + \varphi) - \frac{1}{2}gt^2 + [\dot{y}_i^+ + gt_i + A\omega\cos(\omega t_i + \varphi)](t - t_i) + A\sin(\omega t_i + \varphi) + \frac{1}{2}gt_i^2 + y_i^+ \tag{7}$$

in which $t \in [t_i, t_{i+1}]$, $y_i^+ = y^+(t_i)$ and $\dot{y}_i^+ = \dot{y}^+(t_i)$. Note that the superscript "+" denotes immediately after an impact and likewise, the superscript "−" will be reserved for immediately *before* an impact. The boundary of X_i, ∂X_i constitutes the switch plane of codimension 1 and to study the impact process, we would be interested to obtain the discontinual subset ∂X_{i+1} immediately prior to the $(i+1)$th impact. Therefore, taking values of state variables at $t = t_{i+1}$ in Equation (7) we have:

$$y_{i+1}^- - y_i^+ = -A\sin(\omega t_{i+1} + \varphi) - \frac{1}{2}gt_{i+1}^2 + [\dot{y}_i^+ + gt_i + A\omega\cos(\omega t_i + \varphi)](t_{i+1} - t_i) + A\sin(\omega t_i + \varphi) + \frac{1}{2}gt_i^2. \tag{8}$$

Neglecting the duration of the impact and considering only the simplest impact law, namely, modeling via a constant coefficient of restitution $e \leq 1$, the impact process can be described by

$$y_i^- = y_i^+ = 0 \tag{9}$$

$$\dot{y}_i^+ = -e\dot{y}_i^-. \tag{10}$$

An impact is deemed to occur when Equation (9) is satisfied and the resulting loss of energy is captured by Equation (10). Substituting Equations (9) and (10) into Equations (6) and (8), and replacing y_i^-, $\dot{y}_i^-$ by y_i, $\dot{y}_i$ respectively, to simplify notation usage, we get

$$\dot{y}_{i+1} = -A\omega\cos(\omega t_{i+1} + \varphi) - gt_{i+1} + [-e\dot{y}_i + gt_i + A\omega\cos(\omega t_i + \varphi)] \tag{11}$$

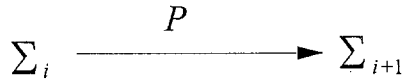

Fig. 2. Mapping diagram for period-1 motion.

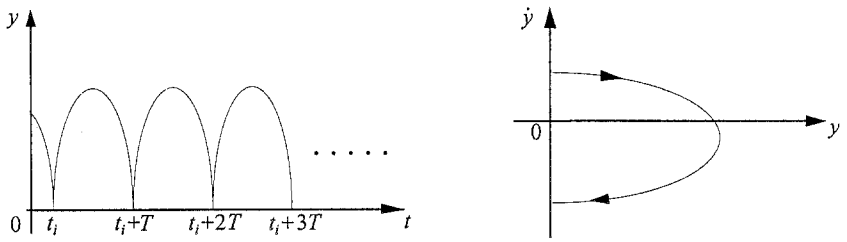

(a) time-displacement (b) phase-plane

Fig. 3. A qualitative sketch of the period-1 physical motion in the relative reference frame.

$$0 = -A\sin(\omega t_{i+1} + \varphi) - \frac{1}{2} g t_{i+1}^2 + [-e\dot{y}_i + g t_i + A\omega\cos(\omega t_i + \varphi)](t_{i+1} - t_i) + A\sin(\omega t_i + \varphi) + \frac{1}{2} g t_i^2. \tag{12}$$

For an impact problem, the discontinual boundary (or switch plane) is the Poincaré mapping section Σ which therefore, can be defined by

$$\Sigma = \bigcup_{i=0}^{N} \Sigma_i, \tag{13}$$

where

$$\Sigma_i = \left\{ (t_i, \dot{y}_i) \;\middle|\; y_i = 0, t_i \bmod \frac{2\pi}{\omega} \right\}. \tag{14}$$

When the absolute reference frame is considered, the Poincaré mapping section is defined by

$$\Sigma_{i(a)} = \left\{ (t_i, \dot{x}_i) \;\middle|\; y_i = 0, t_i \bmod \frac{2\pi}{\omega} \right\}. \tag{15}$$

Note that all quantities measured in the absolute reference frame carry the subscript "a" as shown in Equation (15). The Poincaré mapping P can now be defined as

$$P : \Sigma_i \to \Sigma_{i+1}. \tag{16}$$

Period-1 Motion

In this paper, we considered only the period-1 motion. For this case, the mapping diagram and the physical motion are sketched respectively in Figures 2 and 3. For any $\mathbf{x} = (t_i, \dot{y}_i)^{tp} \in \Sigma$ we have $P\mathbf{x} = \mathbf{x}$, and this leads to the following two equations:

$$t_{i+1} = t_i + \frac{2n\pi}{\omega} = t_i + nT, \qquad n = 1, 2, 3, \ldots \tag{17}$$

$$\dot{y}_{i+1} = \dot{y}_i, \tag{18}$$

where the superscript tp implies transpose (of a matrix) and T is the period of the excitation. Substituting Equations (17) and (18) into Equations (11) and (12) and simplifying yields

$$\dot{y}_i = -\frac{g}{1+e}\frac{2n\pi}{\omega} \tag{19}$$

$$\frac{A\omega^2}{g}\cos(\omega t_i + \varphi) = n\pi\left(\frac{1-e}{1+e}\right). \tag{20}$$

Equations (19) and (20) represent the initial impact conditions for period-1 motion to occur in the repeated impacts of a ball with a massive vibrating table. These are just the necessary conditions and in a later section, we will provide the sufficient conditions as well. Noting that $|\cos(\omega t_i + \varphi)| \leq 1$ in Equation (20) the following more general conditions can be derived:

$$2l\pi - \frac{\pi}{2} \leq \omega t_i + \varphi \leq 2l\pi + \frac{\pi}{2} \tag{21}$$

$$\frac{A\omega^2}{g} \geq n\pi\left(\frac{1-e}{1+e}\right), \tag{22}$$

where l is a positive integer. Note that the impact conditions $(t_i, \dot{y}_i)$ derived here actually represent the fixed points of the discrete mapping, from which the stability of the motion can be ascertained. This is outlined in the next section.

Stability and Bifurcation Conditions

The stability and bifurcation conditions for the period-1 motion are obtained by studying the characteristics of the fixed points of the linearized discrete mapping of Equations (11) and (12):

$$\begin{pmatrix} t_{i+1} \\ \dot{y}_{i+1} \end{pmatrix} = DP \cdot \begin{pmatrix} t_i \\ \dot{y}_i \end{pmatrix} = \left[\frac{\partial P(t_{i+1}, \dot{y}_{i+1})}{\partial(t_i, \dot{y}_i)}\right]\begin{pmatrix} t_i \\ \dot{y}_i \end{pmatrix} = \begin{pmatrix} \frac{\partial t_{i+1}}{\partial t_i} & \frac{\partial t_{i+1}}{\partial \dot{y}_i} \\ \frac{\partial \dot{y}_{i+1}}{\partial t_i} & \frac{\partial \dot{y}_{i+1}}{\partial \dot{y}_i} \end{pmatrix}\begin{pmatrix} t_i \\ \dot{y}_i \end{pmatrix}, \tag{23}$$

where DP is the Jacobian matrix and its elements, $\partial t_{i+1}/\partial t_i$, $\partial t_{i+1}/\partial \dot{y}_i$, $\partial \dot{y}_{i+1}/\partial t_i$, $\partial \dot{y}_{i+1}/\partial \dot{y}_i$, are defined by Equations (A2)–(A5) in the Appendix. Evaluating DP at the fixed points $(t_i, \dot{y}_i)$ by substituting Equations (19) and (20) into Equations (A2)–(A5), we get

$$\frac{\partial t_{i+1}}{\partial t_i} = 1 - \frac{1+e}{g} A\omega^2 \sin(\omega t_i + \varphi) \tag{24}$$

$$\frac{\partial t_{i+1}}{\partial \dot{y}_i} = -\frac{e(1+e)}{g} \tag{25}$$

$$\frac{\partial y_{i+1}}{\partial t_i} = -\frac{1+e}{g}[A\omega^2 \sin(\omega t_i + \varphi)]^2 + (1+e)A\omega^2 \sin(\omega t_i + \varphi) \tag{26}$$

$$\frac{\partial \dot{y}_{i+1}}{\partial \dot{y}_i} = e^2 - A\omega^2 \sin(\omega t_i + \varphi)\frac{e(1+e)}{g}. \tag{27}$$

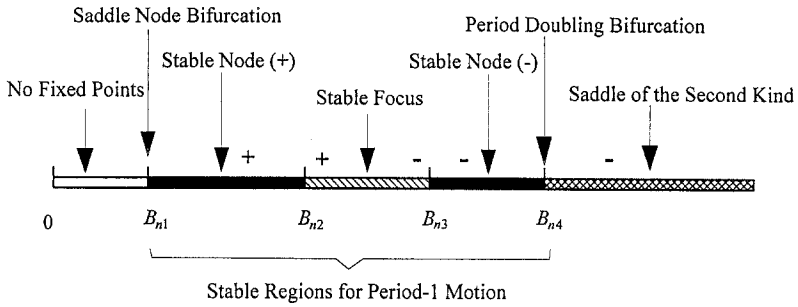

(a) for $\sin(\omega t_i + \varphi) > 0$

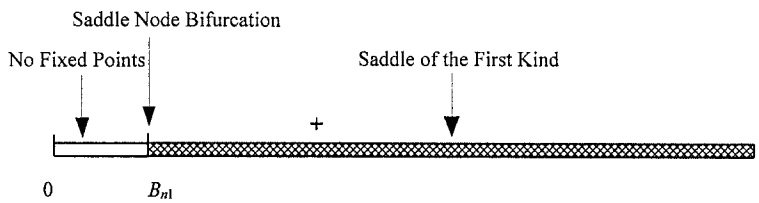

(b) for $\sin(\omega t_i + \varphi) < 0$

Fig. 4. Qualitative analysis of stability and bifurcation for period-1 motion.

The trace and determinant of the Jacobian DP of the mapping are

$$\mathrm{Tr}(DP) = 1 + e^2 - \frac{(1+e)^2}{g} A\omega^2 \sin(\omega t_i + \varphi) \tag{28}$$

$$\mathrm{Det}(DP) = e^2. \tag{29}$$

The eigenvalues λ_1, λ_2 can be computed from

$$\lambda_{1,2} = \frac{\mathrm{Tr}(DP) \pm \sqrt{\mathrm{Tr}(DP)^2 - 4\mathrm{Det}(DP)}}{2}. \tag{30}$$

Stability conditions can be stated as follows: if $|\lambda_1|, |\lambda_2| < 1$, then we have a sink (stable node or focus); if $|\lambda_1| < 1 < |\lambda_2|$, then we have a saddle; and if $|\lambda_1|, |\lambda_2| > 1$, then we have a source. Since $\lambda_1 \cdot \lambda_2 = \mathrm{Det}(DP) = e^2$, only sinks and saddles are found for $e < 1$. For the specific situation of $e = 1$, centers and saddles are obtained. If $|\lambda_j| = 1$ for both eigenvalues, then the norm is preserved in the directions associated with these eigenvalues. Using the stability conditions of the discrete mapping, the stability and bifurcation for period-1 motion can be qualitatively determined as shown in Figure 4. A summary is given as follows.

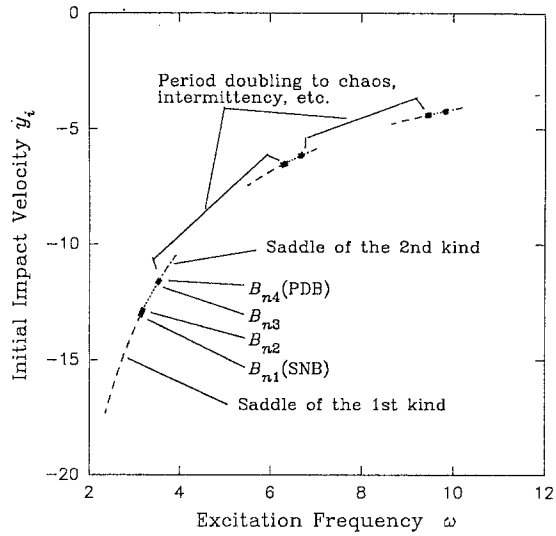

(a) Initial Impact Conditions

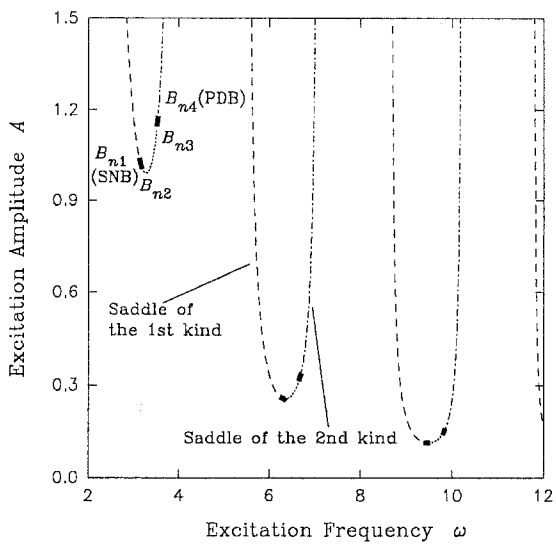

(b) Parameter Manifold

Fig. 5. Quantitative analysis of stability and bifurcation for period-1 motion.

(a) From Figure 4(a), for $\sin(\omega t_i + \varphi) > 0$ (or $2/\pi < \omega t_i + \varphi < 2/\pi + \pi/2$), the parameter range of the stable motion of the bounding ball is

$$B_{n1} < \frac{A\omega^2}{g} < B_{n4} \tag{31}$$

in which the constants $B_{n1}, \ldots, B_{n4}$ in Figure 4 are defined as

$$B_{n1} = n\pi \left(\frac{1-e}{1+e}\right) \tag{32}$$

$$B_{n2} = \frac{1-e}{1+e}\sqrt{\left(\frac{1-e}{1+e}\right)^2 + (n\pi)^2} \tag{33}$$

$$B_{n3} = \sqrt{1 + \left(\frac{n\pi(1-e)}{1+e}\right)^2} \tag{34}$$

$$B_{n4} = \sqrt{\frac{4(1+e^2)^2}{(1+e)^4} + \left(\frac{n\pi(1-e)}{1+e}\right)^2}. \tag{35}$$

REMARKS.

Stable motion:

(i) For $B_{n1} < A\omega^2/g \leq B_{n2}$, the eigenvalues of DP are real and for the range $0 < \lambda_{1,2} < 1$ the fixed point of the mapping is a stable node (+).

(ii) For $B_{n2} < A\omega^2/g \leq B_{n3}$, the eigenvalues of DP are complex conjugate in the range $|\lambda_{1,2}| < 1$. The real part $\mathrm{Re}(\lambda_{1,2})$ changes from positive to negative, and therefore the fixed point of the mapping is a stable focus.

(iii) For $B_{n3} < A\omega^2/g \leq B_{n4}$, eigenvalues of DP are real and for $-1 < \lambda_{1,2} < 0$, the fixed point of the mapping is a stable node (−).

Comparison with Holmes's result [1]:

Holmes [1] presented the following result for the stable motion of the bouncing ball

$$B_{n1} < \frac{A\omega^2}{g} < B_{n3}. \tag{36}$$

Comparing our result in Equation (31) with Holmes's expression in Equation (36), it is clear that the upper limit of the stability condition is different except at $e = 1$. The upper limit of Holmes's result in Equation (36) is just the extreme point of the stable focus (−) as depicted in Figure 4. On the other hand, the upper limit of our result Equation (31) goes a little further, to the point B_{n4} which corresponds to the period-doubling bifurcation condition. We will show through numerical experimentation, that our result is more accurate.

Unstable motion:

The parameter range for the unstable motion of the bouncing ball is given by

$$\frac{A\omega^2}{g} > B_{n4}. \tag{37}$$

For this situation, the eigenvalues $\lambda_{1,2} < 0$ are such that $\lambda_1 < -1 < \lambda_2$, and, therefore, all saddles of the period-1 motion are of the second kind.

(b) From Figure 4(b), for $\sin(\omega t_i + \varphi) < 0$ (or $2/\pi + 3\pi/2 < \omega t_i + \varphi < 2(l+1)\pi$), stable motion cannot exists and thus, we have only the unstable motion which is governed by

$$\frac{A\omega^2}{g} > B_{n1}. \tag{38}$$

This unstable motion is different from the unstable motion in Type (a) and this is evident from its eigenvalues $\lambda_{1,2} > 0$ which are such that $\lambda_1 < 1 < \lambda_2$. That is, for this situation, the fixed

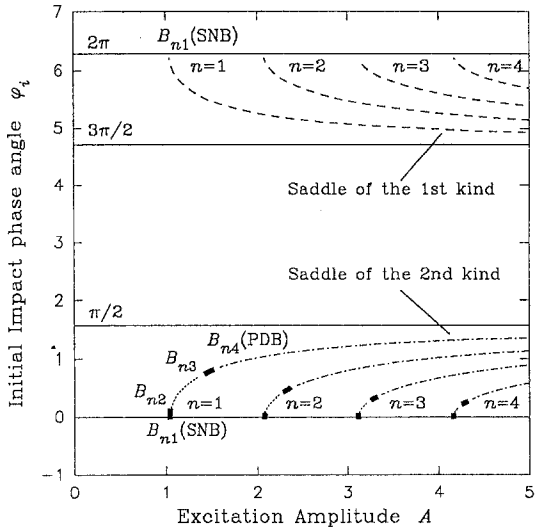

(a) Varying n

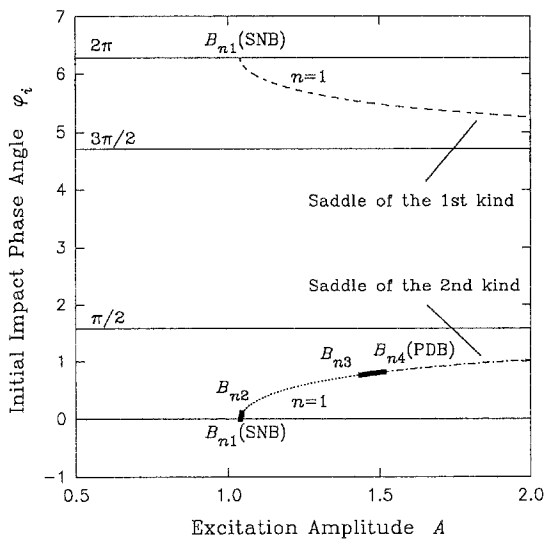

(b) Zoomed View at n=1

Fig. 6. Variation of the initial impact phase angle with the excitation amplitude.

points of period-1 motion are saddles of the first kind.

(c) The bifurcation conditions for period-1 motion of the bouncing ball are:
(i) $A\omega^2/g = B_{n1}$ we have the saddle-node bifurcation, and
(ii) $A\omega^2/g = B_{n4}$ we have the period doubling bifurcation.

These stability and bifurcation conditions are summarized qualitatively in Figure 4. However, it would be much more informative to sketch them quantitatively. We can for example, get a feel for the relative sizes of the stable and unstable regions. The quantitative plots are presented in Figure 5. To generate the plots, the following values are used: $g = 9.8$, $e = 0.5$,

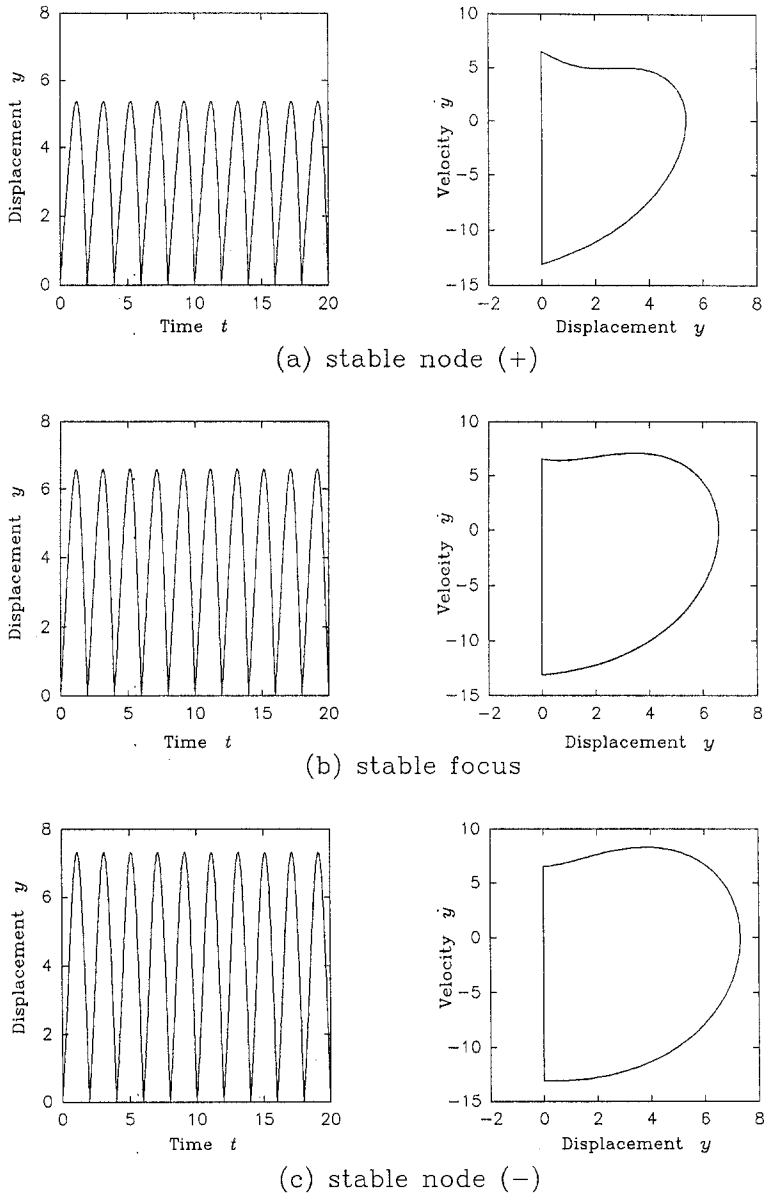

Fig. 7. The three types of stable period-1 motion.

$n = 1$ and $t_i = 2l\pi/\omega + 2 \bmod 2\pi/\omega$. As shown, the dash-line denotes saddle of the first kind; the darkened solid-line, stable node point; the dotted-line, stable focus point; and the dash-dotted-line, saddle of the second kind. To clearly indicate the start/end of the stable regions, $B_{n1}, \ldots, B_{n4}$ are also marked on these graphs. As in Figure 4, B_{n1} in these graphs corresponds to the saddle-node bifurcation (SNB) and likewise, B_{n4} to the period doubling bifurcation (PDB). Note that the *unmarked gaps* between two saddles (including the saddles themselves) represent the period doubling route to chaos, intermittency, etc. We are currently pursuing research to quantitatively chart these gaps.

To provide a comparison with Figure 1 of Holmes [1], Figure 6 is plotted using $g = 9.8$, $e = 0.5$ and $\omega = \pi$. It should be emphasized that the comparison here is qualitative rather than

Table 1. Computed input data for $n = 1$ period-1 motion ($g = 9.8$, $e = 0.5$, $\omega = \pi$, $t_i = 0.0$).

Figure No.	A	$\dot{y}_i$	φ_i	Types of Stability
		Stable Motion		
Figure 9(a)	1.0400639	-13.0666666	0.0219918	Stable node (+)
Figure 9(b)	1.2518871	-13.0666666	0.5966194	Stable focus
Figure 9(c)	1.5039512	-113.066666	0.8073893	Stable node (−)
		Chaotic Motion		
Figure 9(d)	2.0003417	-13.0666666	1.0241592	2nd saddle
Figure 9(e)	2.0003417	-13.0666666	5.2590265	1st saddle

Table 2. Computed input data for $n = 2$ period-1 motion ($g = 9.8$, $e = 0.5$, $\omega = \pi$, $t_i = 0.0$).

Figure No.	A	$\dot{y}_i$	φ_i	Types of Stability
		Stable Motion		
Figure 10(a)	2.0802021	-26.1333332	0.0235619	Stable node (+)
Figure 10(b)	2.1428242	-26.1333332	0.2437340	Stable focus
Figure 10(c)	2.3434676	-26.1333332	0.4790926	Stable node (−)
		Chaotic Motion		
Figure 10(d)	5.0535889	-26.1333332	1.1466812	2nd saddle
Figure 10(e)	5.0535936	-26.1333332	5.1365037	1st saddle

quantitative as it is difficult to obtain the exact values of the parameters used in generating Holmes's solution. For our figures, it is more appropriate to plot them without shifting the graphs by $\pm\pi$ as done by Holmes. Qualitatively, our result compares well with Holmes in the sense that both of them are very similar. However, there is one notable difference. While the start points of the stable regions are the same, the end points are not: Holmes's stable region ends at B_{n3} whereas ours ends at B_{n4}. Also, note that our curves contain additional information pertaining to the nature of the stability which is absent in Holmes's plot.

Numerical Simulations

As a verification of the stability and bifurcation conditions for period-1 motion, numerical simulations are performed. To guarantee stable motion, parametric values are chosen such that they lie within the theoretically determined stable range, and similarly, to simulate unstable motion, parametric values within the theoretically obtained unstable range are used. These computed input parameters for numerical simulations of $n = 1$, period-1 motion are tabulated in Table 1 and, of $n = 2$, period-1 motion in Table 2. For stable motion, we have plotted time-displacement and phase-plane curves based on the equations of motion described by Equations (6)–(7) and (9)–(10) and for unstable motion, we presented Poincaré mapping sections generated via Equations (6)–(7), (9)–(10) and (14)–(15).

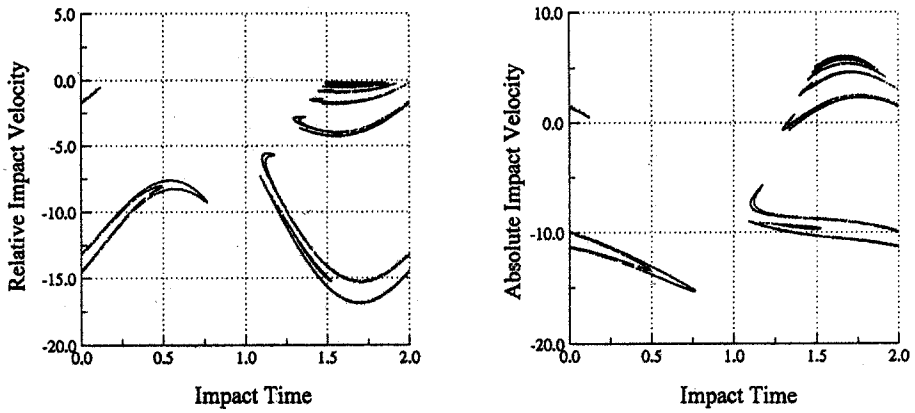

(a) Saddle of the Second Kind

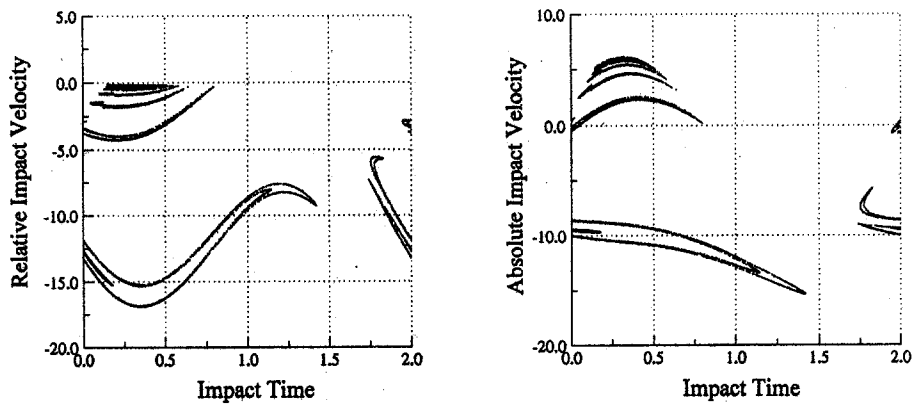

(b) Saddle of the First Kind

Fig. 8. Chaos in the unstable period-1 motion.

Figure 7 depicts the steady period-1 motion of the bouncing ball, in the form of time-displacement and phase-plane curves, corresponding to the three kinds of stability conditions: (a) stable node (+), (b) stable focus and (c) stable node (−). Observe that these three phase-plane curves change their shapes in accordance to the three types of stability, and approach a "D"-shaped curve in (c).

Figure 8 shows the Poincaré mapping sections for the two saddles associated with the period-1 unstable motion. We have plotted the saddle of the second kind ($\sin(\omega t_i + \varphi) \geq 0$) Figure 8(a) and saddle of the first kind ($\sin(\omega t_i + \varphi) \leq 0$) in Figure 8(b). The graphs on the left pertain to the *relative* frame of reference, and on right, to the *absolute* frame of reference. The latter is provided to enable comparisons with physical experiments to be made should these be available. In plotting the two unstable motions, we varied only their phase angles. Observe that when the phase angles are shifted exactly by 2π, we still end up with completely

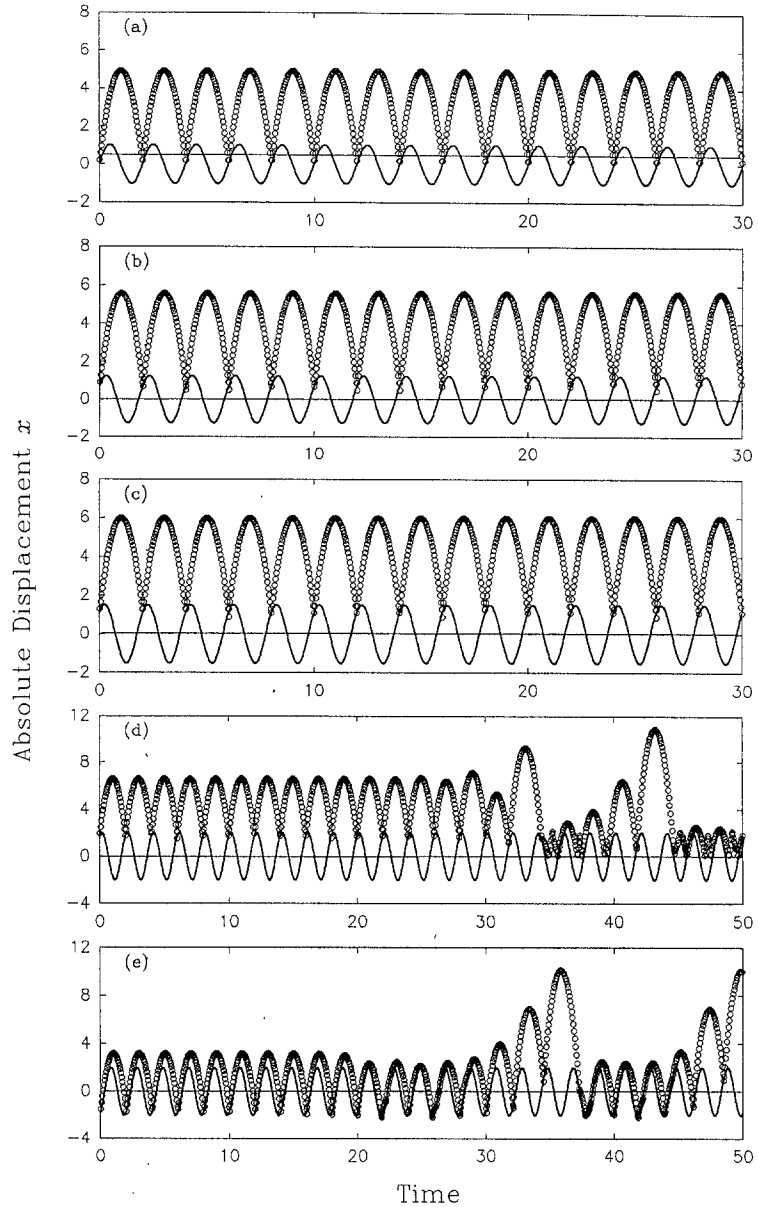

Fig. 9. Period-1 physical motion for $n = 1$. (a) Stable node (+), (b) stable focus, (c) stable node (−), (d) saddle of the second kind and (e) saddle of the first kind; o o o ball, ——— table.

identical Poincaré mapping sections. What this implies is that the two saddles have *identical* Smale horseshoe structure. Furthermore, a careful scrutiny of Figure 8 reveals that there exists self-similarity, indicating the presence of fractals. Thus, a chaotic attractor is clearly evident in the plot for the parameters chosen.

It would be very interesting to view the physical motion of the bouncing ball. This illustrated in Figure 9 and 10, superimposed together with the physical motion of the vibrating table for up to $t = 50$ s. Both stable and unstable motion are drawn. Since Holmes's model is based on a discrete mapping, he can only furnish a qualitative sketch and only for the stable motion. In contrast, based on our differential equation model, we can produce a quantitative

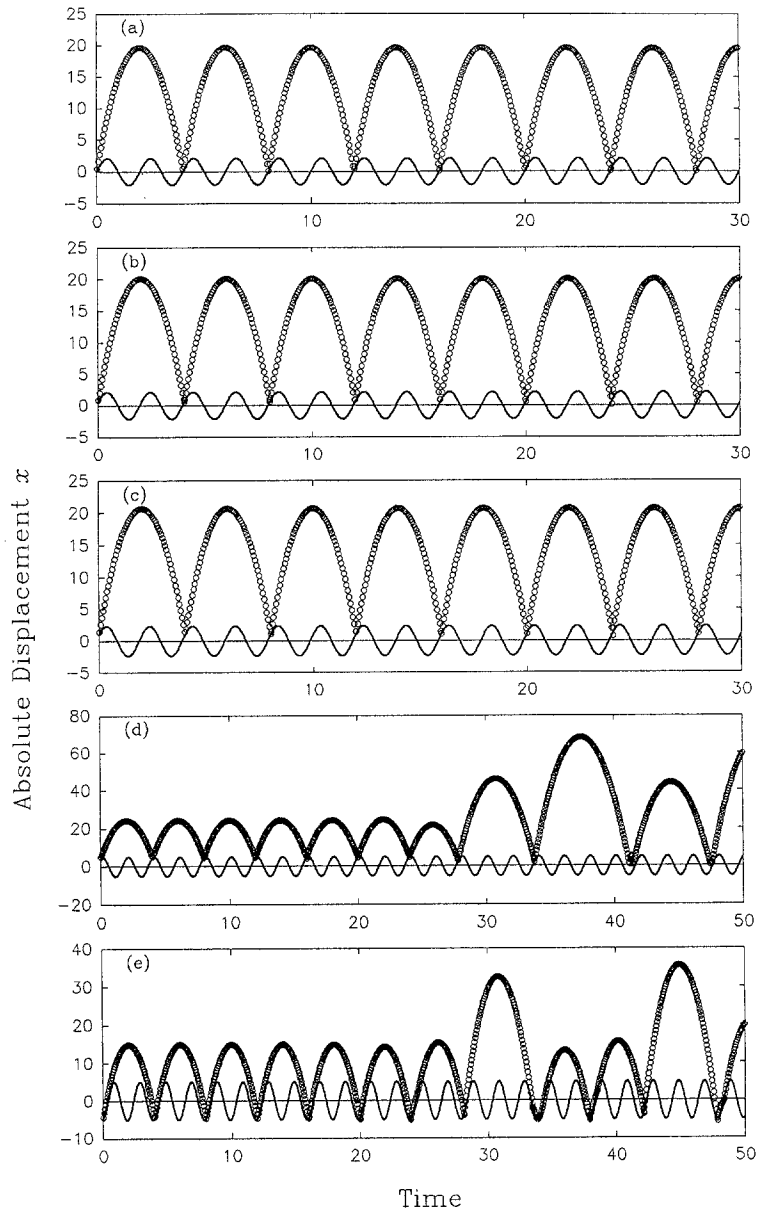

Fig. 10. Period-1 physical motion for $n = 2$. (a) Stable node (+), (b) stable focus, (c) stable node (−), (d) saddle of the second kind and (e) saddle of the first kind; o o o ball, ——— table.

description of the physical motion of the bouncing ball, for stable and as well as unstable motion. Note that for both Figures 9 and 10, the following graphs are plotted: (a) stable node (+), (b) stable focus, (c) stable node (−), (d) saddle of the second kind and (e) saddle of the first kind. Motions (a)–(c) are stable whereas (d)–(e) are chaotic. In Figure 9, the $n = 1$ motion is generated and in Figure 10, the $n = 2$ motion is produced.

In addition to the analytical checks presented in the previous section, we can also demonstrate physically that the motion in Figures 9 and 10(d)–(e) are indeed chaotic, by simulating the physical motion over a prolonged period of time and checking if they would repeat them-

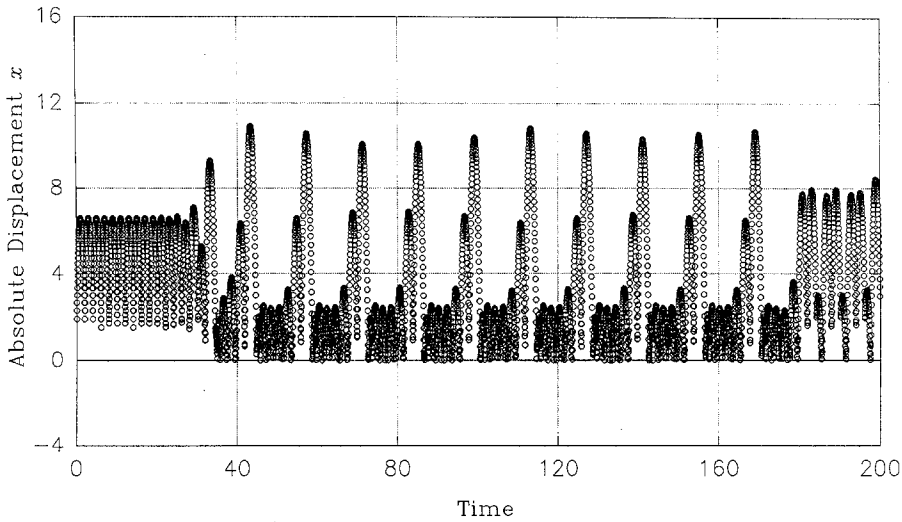

(a) Saddle of the Second Kind

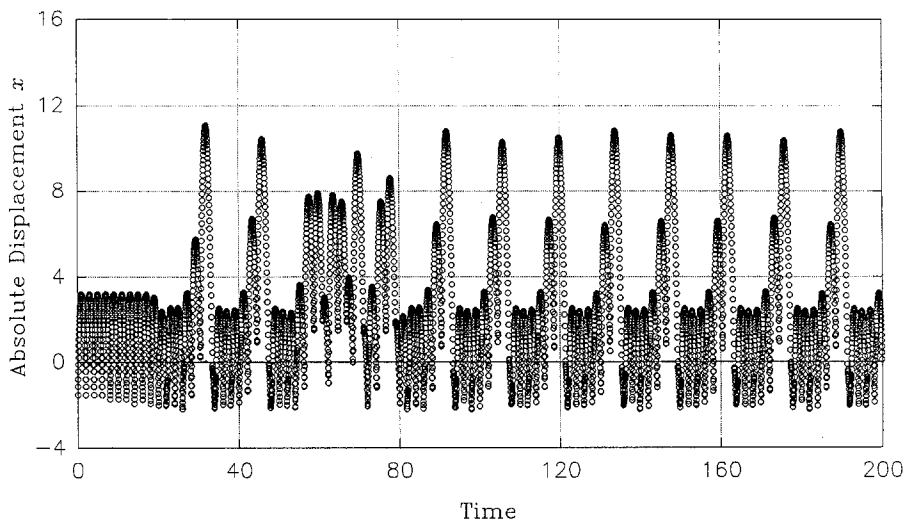

(b) Saddle of the First Kind

Fig. 11. Extended period-1 physical motion for $n = 1$ (table motion not shown).

selves. The results are shown in Figures 11 and 12 where the unstable motion is re-plotted for up to $t = 200$ s. Observe that the motions do not repeat themselves for this duration of time.

Conclusions

The dynamics of a bouncing ball with a sinusoidally vibrating table is revisited in this work. Based on the equation of motion, the mapping for period-1 motion of the ball is constructed. The stability and bifurcation conditions for this motion are derived and compared with those

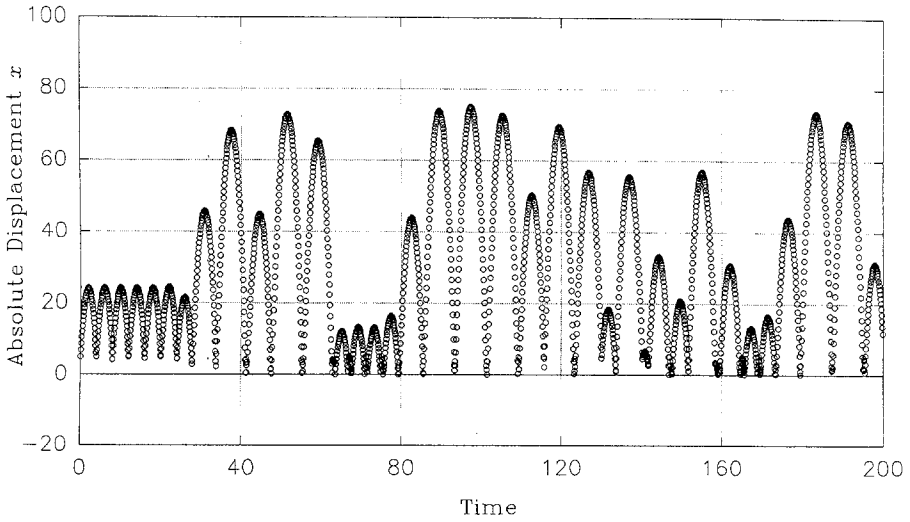

(a) Saddle of the Second Kind

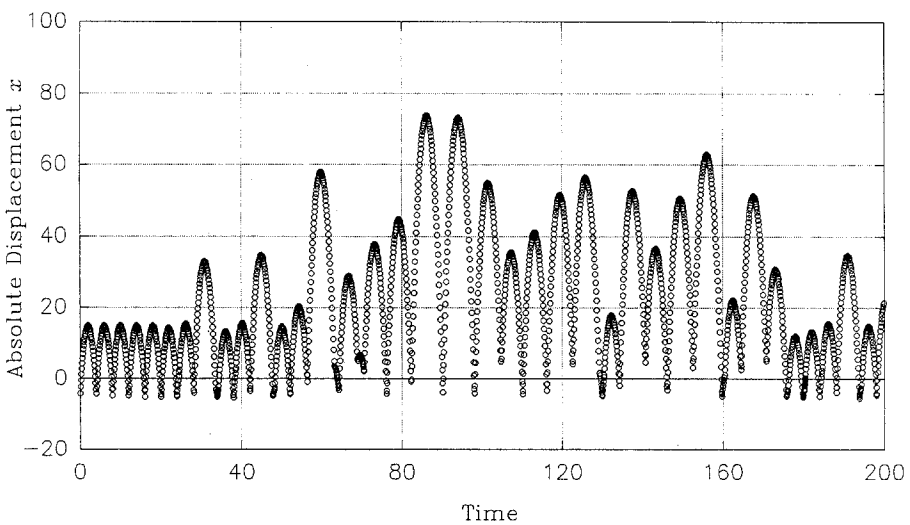

(b) Saddle of the First Kind

Fig. 12. Extended period-1 physical motion for $n = 2$ (table motion not shown).

of Holmes [1]. For period-1 motion, three kinds of stable motion exist: stable node (+), stable focus and stable node (−), and for the unstable motion, we have two types: saddle of the first kind and saddle of the second kind. It is found that Holmes's range of stable motion is narrower than ours, and through numerical simulations, our result is shown to be more accurate. Also, from the Poincaré mapping sections of the unstable motion, the two saddles have identical Smale horseshoe structures and possess the self-similarity character. Thus, the unstable motion is indeed chaotic. Plots of the physical motion of the bouncing ball superimposed on the vibration of the table are also given. The result is consistent with the nature of the motion. For stable physical motion, it is periodic and for unstable physical

motion (i.e. chaotic motion), it does not repeat itself even when simulated for an extended period of time.

Acknowledgement

Financial supports in the form of a research grant from the Natural Science and Engineering Research Council of Canada (NSERC) and a University of Manitoba doctoral fellowship to the first author are gratefully acknowledged.

Appendix: Stability and Bifurcation

The Jacobian of mapping P at the ith impact of the bouncing ball, DP is defined as

$$DP = \left[\frac{\partial P(t_{i+1}, \dot{y}_{t+1})}{\partial t_i, \dot{y}_i})\right] = \begin{pmatrix} \frac{\partial t_{i+1}}{\partial t_i} & \frac{\partial t_{i+1}}{\partial \dot{y}_i} \\ \frac{\partial \dot{y}_{i+1}}{\partial t_i} & \frac{\partial \dot{y}_{i+1}}{\partial \dot{y}_i} \end{pmatrix}_{(t_i, \dot{y}_i)}, \tag{A1}$$

where

$$\frac{\partial t_{i+1}}{\partial t_i} = \frac{1}{\dot{y}_{i+1}}\{-e\dot{y}_i + [A\omega^2 \sin(\omega t_{i+1} + \varphi) - g](t_{i+1} - t_i)\} \tag{A2}$$

$$\frac{\partial t_{i+1}}{\partial \dot{y}_i} = \frac{e}{\dot{y}_{i+1}}(t_{i+1} - t_i) \tag{A3}$$

$$\frac{\partial \dot{y}_{i+1}}{\partial t_i} = [A\omega^2 \sin(t_{i+1} + \varphi) - g]\frac{\partial t_{i+1}}{\partial t_i} - [A\omega^2 \sin(t_i + \varphi) - g] \tag{A4}$$

$$\frac{\partial \dot{y}_{i+1}}{\partial \dot{y}_i} = [A\omega^2 \sin(\omega t_{i+1} + \varphi) - g]\frac{\partial t_{i+1}}{\partial \dot{y}_i} - e. \tag{A5}$$

For any period-k motion of the bouncing ball, we have $\mathbf{x}_{i+k} = P^{(k)}\mathbf{x}_i$, where $P^{(k)} = \underbrace{P \circ P \circ \cdots \circ P}_{k}$. Its Jacobian at the fixed point is

$$\begin{aligned} DP^{(k)} &= \underbrace{DP \bullet \cdots \bullet DP}_{k} \\ &= \left[\frac{\partial P(t_{i+k}, \dot{y}_{i+k})}{\partial(t_{i+k-1}, \dot{y}_{i+k-1})}\right] \cdots \left[\frac{\partial P(t_{i+1}, \dot{y}_{i+1})}{\partial(t_i, \dot{y}_i)}\right]_{\binom{t_{i+k}}{\dot{y}_{i+k}} = \binom{(2n\pi/\omega)+t_i}{\dot{y}_i}} \end{aligned} \tag{A6}$$

from which the trace $\mathrm{Tr}(DP^{(k)})$ and determinant $\mathrm{Det}(DP^{(k)})$ of Equation (A6) can be easily evaluated. The eigenvalues can be computed from

$$\lambda_{1,2} = \frac{\mathrm{Tr}(DP^{(k)}) \pm \sqrt{\mathrm{Tr}(DP^{(k)})^2 - 4\mathrm{Det}(DP^{(k)})}}{2}. \tag{A7}$$

The condition for period doubling bifurcation of the period-k motion of the ball is

$$\mathrm{Tr}(DP^{(k)}) + \mathrm{Det}(DP^{(k)}) + 1 = 0 \tag{A8}$$

and likewise, the condition for saddle node bifurcation of the period-k motion of the ball is

$$\mathrm{Tr}(DP^{(k)}) = 1 + \mathrm{Det}(DP^{(k)}). \tag{A9}$$

References

1. Holmes, P. J., 'The dynamics of repeated impacts with a sinusoidally vibrating table', *Journal of Sound and Vibration* **84**, 1982, 173–189.
2. Guckenheimer, J. and Holmes, P. J., *Nonlinear Oscillations, Dynamical Systems, and Bifurcation of Vector Fields*, Springer-Verlag, New York, 1983.
3. Wood, L. A. and Byrne, K. P., 'Analysis of a random repeated impact process', *Journal of Sound and Vibration* **81**, 1981, 329–325.
4. Everson, R. M., 'Chaotic dynamics of a bouncing ball', *Physica D* **19**, 1986, 355–383.
5. Masri, F. and Caughey, T. K., 'On the stability of the impact damper', *ASME Journal of Applied Mechanics* **33**, 1966, 587–592.
6. Shaw, S. W. and Holmes, P. J., 'A periodically forced piecewise linear oscillator', *Journal of Sound and Vibration* **90**, 1983, 123–155.
7. Reithmeier, E., 'Periodic solutions on nonlinear dynamical systems with discontinuities', in *Proceedings of the IUTAM Symposium on Nonlinear Dynamics in Engineering Systems*, Stuttgart, 1989, pp. 249–256.
8. Han, R. P. S., Luo, A. C. J., and Deng, W., 'Chaotic motion of a horizontal impact pair', *Journal of Sound and Vibration* **181**, 1995, 231–250.
9. Bapat, C. N. and Bapat, C., 'Impact-pair under periodic excitation', *Journal of Sound and Vibration* **120**, 1987, 53–61.
10. Heiman, M. S., Sherman, P. J., and Bajaj, A. K., 'On the dynamics and stability of an inclined impact pair', *Journal of Sound and Vibration* **114**, 1987, 535–547.
11. Heiman, S., Bajaj, A. K., and Sherman, P. J., 'Periodic motions and bifurcation in dynamics of an inclined impact pair', *Journal of Sound and Vibration* **124**, 1988, 55–78.
12. Shaw, J. and Shaw, S. W., 'The onset of chaos in a two degree-of-freedom impact system', *ASME Journal of Applied Mechanics* **56**, 1989, 168–174.
13. Bayly, V. and Virgin, L. N., 'An experimental study of an impacting pendulum', *Journal of Sound and Vibration* **164**, 1993, 364–374.
14. Whiston, G. S., 'Singularities in vibro-impact dynamics', *Journal of Sound and Vibration* **152**, 1992, 427–460.
15. Peterka, F. and Vacik, J., 'Transition to chaotic motion in mechanical systems with impacts', *Journal of Sound and Vibration* **154**, 1992, 95–115.
16. Han, R. P. S. and Luo, A. C. J., 'Period-n motion of a bouncing ball with a harmonically excited table', in preparation.